AJNR

Improved Delineation of Arteries in the Posterior Fossa of the Brain by Model-Based Iterative Reconstruction in Volume-Rendered 3D CT Angiography

H. Machida, H. Takeuchi, I. Tanaka, R. Fukui, Y. Shen, E. Ueno, S. Suzuki and X.-Z. Lin

Improved Delineation of Arteries in the Posterior Fossa of the Brain by Model-Based Iterative Reconstruction in Volume-Rendered 3D CT Angiography

H. Machida, H. Takeuchi, I. Tanaka, R. Fukui, Y. Shen, E. Ueno, S. Suzuki, and X.-Z. Lin

ABSTRACT

BACKGROUND AND PURPOSE: Improved CTA delineation of arteries and unruptured aneurysms is clinically desired in the posterior fossa. We present a novel model-based iterative reconstruction that models system statistics and optics to improve CT image quality. We investigated the utility of MBIR for improving delineation of arteries in the posterior fossa on 3D brain CTA.

MATERIALS AND METHODS: Using filtered back-projection with a standard kernel and MBIR, we reconstructed axial images of 0.625-mm thickness of 28 consecutive patients (14 men; mean age, 58.6 ± 14.6 years) who underwent 64-detector brain CTA. We placed regions of interest on the axial images, measured the mean CT value in the basilar artery and the value and SD in the pons and bilateral cerebellar hemispheres, and calculated the contrast-to-noise ratio of the brain arteries in the posterior fossa. Using volume-rendered CTA and a 4-point scale, 2 radiologists independently graded delineation of the BA, bilateral vertebral artery, superior cerebellar artery, and anterior and posterior inferior cerebellar arteries. We compared the results between FBP and MBIR by using paired t and Wilcoxon signed-rank tests.

RESULTS: Compared with FBP, MBIR significantly improved the contrast-to-noise ratio ($P < .0001$) and subjective delineation of all arteries in the posterior fossa except the BA (VA, SCA, AICA, and PICA; $P < .05$ for all). The mean visual score by MBIR was 3.0 or higher for all those arteries except the AICA assessed by reader 1 (2.6 ± 0.7).

CONCLUSIONS: With 3D brain CTA, contrast-to-noise ratio and arterial delineation of the VA, SCA, AICA, and PICA in the posterior fossa are better with MBIR than FBP.

ABBREVIATIONS: AICA = anterior inferior cerebellar artery; BA = basilar artery; FBP = filtered back-projection; MBIR = model-based iterative reconstruction; SCA = superior cerebellar artery; VA = vertebral artery

The standard filtered back-projection algorithm with CT assumes perfect projection samples by ignoring the noise inherent in x-ray attenuation and detector electronics and assumes ideal system optics by featuring point sources, voxels, and detector elements. Model-based iterative reconstruction, a clinically available state-of-the-art comprehensive algorithm for CT, models system noise statistics and 3D system optics of the specific CT scanner hardware for which it was developed. Phantom studies have confirmed enhanced image resolution, lower noise, and re-duced helical conebeam artifacts by using the MBIR algorithm.[1] Thus, its use is expected to improve image quality and enable reduced doses of radiation and contrast medium in CT studies in various clinical fields.

3D CT angiography can be used to guide the treatment strategy by permitting precise assessment of the size and shape of intracranial aneurysms and their anatomic relationships with parent vessels.[2-6] Especially, the use of the volume-rendered technique maintains the original anatomic spatial relationships of the CT dataset and offers a 3D perspective to facilitate interpretation of vascular interrelationships. At least 10% of unruptured intracranial aneurysms occur in the vertebrobasilar system, a location reported to be a significant independent predictor of aneurysm rupture.[7,8] On the other hand, posterior fossa artifacts and enhanced image noise can hinder delineation of those aneurysms. Thus, we compared delineation of the arteries in the posterior fossa and vertebrobasilar system on volume-rendered 3D CTA between MBIR and FBP to assess whether MBIR achieved more useful results.

MATERIALS AND METHODS

Study Population

From March 10 through April 7, 2011, we retrospectively evaluated images of 28 consecutive patients (14 men, 14 women; 26–80 years of age; mean age, 58.6 ± 14.6 years) who underwent CTA of the brain arteries by using a garnet-based 64-detector high-definition CT scanner (Discovery CT750 HD; GE Healthcare, Milwaukee, Wisconsin) and our standard protocol. The CTA examinations were performed for further evaluation of unruptured intracranial aneurysms (14 patients), intracerebral hemorrhage ($n = 4$), subarachnoid hemorrhage ($n = 3$), cerebral infarction ($n = 3$), and Moyamoya disease ($n = 1$) and after coil embolization for saccular aneurysms of the internal carotid artery ($n = 3$). Tokyo Women's Medical University institutional review board waived informed patient consent for this retrospective study, but all patients provided written informed consent for the CTA examinations.

Image Data Acquisition

To minimize motion artifacts, patients underwent CTA examination with their heads immobilized by using a head holder. For the contrast-enhanced helical CT scan, parameters were the following: tube voltage, 120 kV; tube current, 335 mA; rotation speed, 0.5 seconds; and pitch, 0.516. Patients received a bolus of contrast medium with iodine concentration of 370 mgI/mL (50 mL of iopamidol; Iopamiron, Bayer HealthCare, Osaka, Japan) via a 20-ga intravenous catheter placed in an antecubital vein at a rate of 4.0 mL/s followed by a 30-mL saline bolus at the same rate by using a double-head power injector (Dual Shot, type GX; Nemoto Kyorindo, Tokyo, Japan). To determine the scanning delay, a test bolus of 10 mL of contrast medium and 15 mL of saline was injected at the same rate. For each patient, a circular region of interest was placed within the A1/A2 portion of the anterior cerebral artery to determine the peak time of attenuation, and the CT scan was started 2 seconds after that peak. The patient underwent scanning in the craniocaudal direction from the top of the cranial vault to the bottom of the anterior arch of the first cervical vertebra. Helical data were reconstructed in the axial plane (FOV, 20 cm) with a section thickness of 0.625 mm at 0.625-mm intervals using FBP with a standard kernel (matrix size, 512 × 512) and MBIR (matrix size, 1024 × 1024) and then were transferred to a workstation (Advantage Windows 4.5; GE Healthcare). This MBIR algorithm (Veo; GE Healthcare) was clinically available for cranial CT or CTA examinations only with a matrix size of 1024 × 1024.

On the workstation, 2 trained radiology technologists generated volume-rendered 3D CTA images by using a standard technique. The same parameters for volume-rendered reconstruction were used for all patients and both reconstruction algorithms: a linear threshold with a lower threshold value of 125 HU set at 0% opacity (completely transparent) and an upper threshold of 600 HU set at 100% opacity (completely opaque). Bone structures were not edited out of the axial images. The 3D CTA images of the posterior fossa of each patient were extracted by using an 8-cm FOV and were displayed in a view from behind with superoinferior angulation of approximately 30°; for comparison, identical images reconstructed by FBP and MBIR were arranged side by side on the workstation.

Quantitative Assessment

For each patient, the 2 radiology technologists placed circular ROIs of uniform size within the pons, bilateral cerebellar hemispheres, and basilar artery on the reconstructed axial images of 0.625-mm thickness to measure the attenuation value and its SD with the 2 different reconstruction algorithms. For each reconstruction method, we calculated the mean attenuation value of the BA; used the averaged attenuation value in the pons and bilateral cerebellar hemispheres as the attenuation value in posterior fossa, and the averaged SD value in the pons and bilateral cerebellar hemispheres as the objective noise in the posterior fossa and calculated the contrast-to-noise ratio as contrast-to-noise ratio = (attenuation value in BA − attenuation value in posterior fossa) / objective noise in posterior fossa.

We recorded the volume CT dose index (measured in milligrays) and dose-length product (measured in milligrays × centimeter) displayed on the dose report on the CT scanner for each patient and calculated the mean volume CT dose index and dose-length product in our patients.

Qualitative Assessment

Two board-certified radiologists experienced in interpreting CTA of the brain with 8 and 13 years' cumulative experience (H.T. [reader 1] and H.M. [reader 2]), respectively, and blinded to information about patients and reconstruction methods independently performed visual evaluation of not only volume-rendered but also coronal maximum-intensity-projection CTA images of each patient in the posterior view obtained by using the 2 different reconstruction algorithms and displayed side by side at the workstation. For the maximum-intensity-projection reconstruction, they used the same parameters for all patients and both reconstruction algorithms (slab thickness, 10 mm; FOV, 8 cm; window level, 300 HU; and window width, 900 HU) and viewed these images while scrolling. They focused on delineation of the arteries in the posterior fossa: the BA and bilateral vertebral artery and their branches, the bilateral superior cerebellar artery, and the anterior and posterior inferior cerebellar arteries. Visual evaluation was generally performed at a fixed view, with the viewing direction adjusted only to avoid superimposition of vessels and to confirm anatomy, if necessary. They scored the images on a 4-point scale (4, excellent; 3, good; 2, fair; 1, poor) with regard to vessel depiction and contrast, superimposed image noise, and sharpness of vessel contour. Scores of 2, 3, and 4 represented acceptable image quality, and a score of 1 point, unacceptable quality.

Statistical Analysis

All continuous variables were expressed as mean ± SD. We performed statistical analysis by using StatView for Windows (Version 5.0; SAS Institute, Cary, North Carolina). We used a paired t test to compare objective results and the Wilcoxon signed-rank test to compare subjective results between the FBP and MBIR reconstruction algorithms. We assessed inter-reader agreement of the visual evaluation scores by using Cohen κ statistics. $P < .05$ was considered statistically significant.

RESULTS

Quantitative Results

The mean volume CT dose index was 56.2 ± 0.1 mGy, and the mean dose-length product, 983.7 ± 50.2 mGy × cm, based on the imaging parameters for 3D CT angiography of the brain arteries.

Table 1: Quantitative assessment[a]

	FBP	MBIR	P Value
BA attenuation (HU)	422.0 ± 93.3	466.1 ± 90.5	<.0001
Image noise (HU)	10.1 ± 1.3	8.8 ± 0.7	<.0001
CNR	37.9 ± 11.0	48.2 ± 10.1	<.0001

Note:—CNR indicates contrast-to-noise ratio.
[a] Data are means.

Table 1 summarizes the results of quantitative assessment. MBIR significantly improved the attenuation value of the BA, image noise, and contrast-to-noise ratio (466.1 ± 90.5 HU, 8.8 ± 0.7 HU, and 48.2 ± 10.1) compared with FBP (422.0 ± 93.3 HU, 10.1 ± 1.3 HU, and 37.9 ± 11.0) ($P < .0001$ for all).

Qualitative Results

Table 2 summarizes the results of the qualitative assessment.

On volume-rendered images, the mean visual evaluation score by both readers decreased in order from the BA and VA to the PICA to the SCA to the AICA by using both FBP and MBIR algorithms. The scores for the BA and VA by MBIR were 3 or 4 for both readers in all patients and by FBP in 27 of 28 patients (96%). Compared with FBP, MBIR significantly improved subjective delineation of all brain arteries in the posterior fossa except the BA (SCA, AICA, and PICA: $P < .0001$ for both the readers; VA: $P = .046$ [reader 1] and $P = .008$ [reader 2]). The mean visual score by MBIR was 3.0 or higher for all those arteries except the AICA as assessed by reader 1 (2.6 ± 0.7). Image quality was acceptable (score 2, 3, or 4) for most arteries in the posterior fossa by MBIR; Reader 1 scored only 1 SCA image as unacceptable. The interreader agreement of the visual scores was moderate (κ value, 0.43 [95% confidence interval, 0.36–0.50]).

On maximum intensity projections, the mean visual evaluation score by both readers decreased in order from the BA and VA to the SCA and PICA to the AICA by using both FBP and MBIR algorithms. Compared with FBP, MBIR significantly improved subjective delineation of all brain arteries, particularly larger arteries such as the BA and VA, in the posterior fossa ($P < .0001$ for both the readers). The averaged improvement of the visual score by MBIR compared with FBP was 0.84 for the BA and VA and 0.46 for the SCA, AICA, and PICA. The mean visual score by MBIR was 3.0 or higher for all those arteries except the AICA (2.8 ± 0.7 by both the readers), whereas the score by FBP was 3.0 or higher only for the BA and VA. Image quality was acceptable for all the arteries in the posterior fossa by both FBP and MBIR. The interreader agreement of the visual scores was substantial (κ value, 0.75 [95% confidence interval, 0.69–0.81]).

In images of the posterior fossa in a 69-year-old woman with a basilar apex aneurysm, volume-rendered 3D CTA by using the 2 different reconstruction algorithms demonstrated particularly improved delineation of the bilateral AICA and SCA by MBIR compared with FBP, with comparable delineation of the BA and bilateral VA between the 2 algorithms (Fig 1). On maximum intensity projections, MBIR improved subjective delineation of all brain arteries in the posterior fossa, including the BA, with improved vessel enhancement and sharpness of vessel contour, compared with FBP (Fig 1).

DISCUSSION

At least 10% of unruptured intracranial aneurysms occur in the vertebrobasilar system, a location reported as a significant independent predictor of aneurysm rupture.[7,8] Many aneurysms in this location are detected only after ≥2 digital subtraction angiography studies.[9-11] BA aneurysms masked by crossflow phenomena and peripherally located aneurysms of the posterior fossa with reduced filling flow can frequently be overlooked at the first DSA study. Peripherally located aneurysms of the posterior fossa are not rare,[12] but some can be detected only with brain CTA.[13,14] Volume-rendered 3D CTA can provide complete quantification and characterization of intracranial aneurysms and important information for treatment planning.[2-6]

Increased image noise and artifacts can degrade CTA delineation of brain arteries, especially small vessels, in the posterior fossa.[15,16] Use of higher spatial resolution to improve small-vessel depiction leads to increased noise; use of higher tube current to reduce noise increases radiation exposure; use of a high dose of contrast to improve arterial enhancement and thus the contrast-to-noise ratio may increase the risk of contrast-induced nephropathy in patients with marginal renal function; and a rapid injection rate increases the risk of extravasation at the injection site. In large part, posterior fossa artifacts represent beam-hardening artifacts and nonlinear partial volume effects caused by the thick irregular bone of the skull base.[17-19] Previous studies have used a variety of technologies to decrease these artifacts, including the use of newer multidetector CT machines using a helical scan technique with thinner image collimation, higher output tubes, and better reconstruction algorithms (such as beam-hardening correction and iterative reconstruction).[16-18,20-23] The polychromaticity of x-rays causes beam-hardening artifacts in images and loss of information from energy averaging, but monochromatic images produced with CT spectral imaging have recently been reported to reduce beam-hardening artifacts and image noise in the posterior fossa.[24] On the other hand, iterative reconstruction can recover the attenuation map[23] and was confirmed to be robust and effective for beam-hardening correction.[25]

MBIR is a comprehensive state-of-the-art iterative algorithm for image reconstruction for clinical CT study that has the potential to improve image quality with respect to noise, spatial resolution, and helical conebeam artifacts[1] and to reduce radiation and the contrast-medium dose, with only the sacrifice of a long computing time in the present state. Specifically, the average reconstruction time for CTA of the brain with MBIR was approximately 1 hour in this study. Different from FBP, MBIR models the statistical behavior of measurements (photon statistics and electronic noise) and detector response to incident photons (system optics). The latter model describes how each element of the object illuminated by x-ray from the source is projected onto the detector. Each voxel element of the scanned object is represented by a finite 3D volume, and voxels are illuminated by a finite beam that stems from a focal spot of known dimensions and that is measured over the active area of the detector. This spatially varying behavior better models the real CT system than the point model of FBP and leads to better information recovery in the CT image.

In phantom experiments, MBIR achieved only slightly lower through-plane resolution than FBP with half the detector aper-

Table 2: Qualitative assessment[a]

	VR			MIP		
	FBP	MBIR	P Value	FBP	MBIR	P Value
BA (reader 1)	3.9 ± 0.4	4.0 ± 0.2	.083	3.0 ± 0.3	3.8 ± 0.4	<.0001
BA (reader 2)	3.9 ± 0.3	4.0 ± 0.0	.083	3.0 ± 0.2	3.9 ± 0.3	<.0001
VA (reader 1)	3.9 ± 0.3	4.0 ± 0.1	.046	3.0 ± 0.2	3.7 ± 0.5	<.0001
VA (reader 2)	3.9 ± 0.3	4.0 ± 0.0	.008	3.0 ± 0.0	3.9 ± 0.4	<.0001
SCA (reader 1)	2.1 ± 0.7	3.0 ± 0.6	<.0001	2.8 ± 0.5	3.1 ± 0.6	<.0001
SCA (reader 2)	2.5 ± 0.9	3.6 ± 0.7	<.0001	2.8 ± 0.4	3.4 ± 0.7	<.0001
AICA (reader 1)	1.6 ± 0.7	2.6 ± 0.7	<.0001	2.4 ± 0.5	2.8 ± 0.7	<.0001
AICA (reader 2)	1.7 ± 0.9	3.2 ± 0.9	<.0001	2.4 ± 0.5	2.8 ± 0.7	<.0001
PICA (reader 1)	2.7 ± 0.6	3.3 ± 0.5	<.0001	2.7 ± 0.5	3.3 ± 0.6	<.0001
PICA (reader 2)	2.9 ± 0.8	3.8 ± 0.4	<.0001	2.8 ± 0.4	3.3 ± 0.7	<.0001

Note:—VR indicates volume-rendered; MIP, maximum intensity projection.
[a] Data are means.
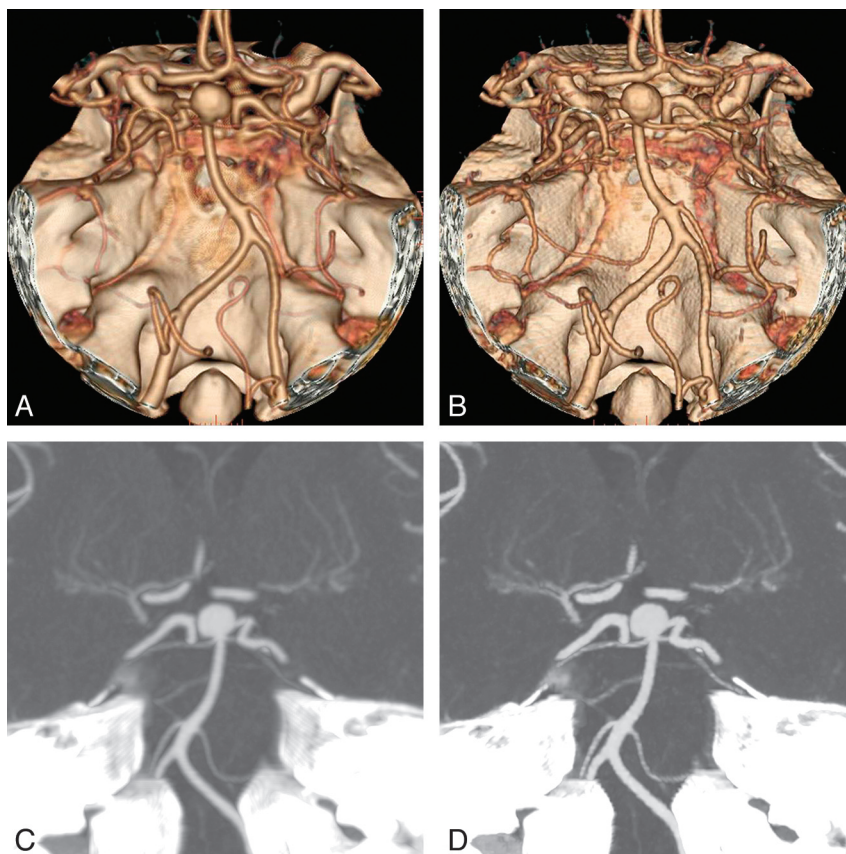
FIG 1. A 69-year-old woman with a basilar apex aneurysm. Volume-rendered (VR) 3D CTAs of the posterior fossa by using 2 different reconstruction algorithms, filtered back-projection (FBP) with a "standard" kernel (A) and model-based iterative reconstruction (MBIR) (B), and oblique coronal maximum-intensity-projection (MIP) CTAs by using FBP with a "standard" kernel (C) and MBIR (D). On VR, delineation of the bilateral anterior inferior cerebellar (AICA) and superior cerebellar (SCA) arteries is particularly improved by MBIR compared with FBP (reader 1: right AICA, 3 versus 3; left AICA, 3 versus 2; and bilateral SCA, 2 versus 2; reader 2: right AICA, 4 versus 3; left AICA, 4 versus 1; right SCA, 4 versus 2; and left SCA, 3 versus 2); and delineation of the basilar (BA) and bilateral vertebral arteries (VA) is comparable between the 2 algorithms (readers 1 and 2: the BA and bilateral VA, 4 versus 4). On MIP, delineation of the BA (readers 1 and 2: four versus 3) and the AICA (reader 1: right AICA, 4 versus 3; left AICA, 3 versus 3; reader 2: right AICA, 3 versus 3; left AICA, 3 versus 2) and SCA (reader 1: right SCA, 3 versus 2; left SCA, 2 versus 2; reader 2: right SCA, 4 versus 3; left SCA, 3 versus 2) is improved by MBIR compared with FBP.

order from "standard" to "detail" to "bone." Thus, by affecting image noise and spatial resolution, MBIR can improve high- and low-contrast resolution. In addition, MBIR can reduce helical artifacts, including blurring, shading, and windmill artifacts.[1]

The MBIR algorithm that we used in this study was clinically available for cranial CT or CTA examinations only, with a matrix size of 1024 × 1024, which also contributed to the increased spatial resolution by MBIR compared with FBP, with a matrix size of 512 × 512. Nevertheless, MBIR significantly improved objective image noise compared with FBP.

The mean diameter of the normal basilar artery is 3.17 mm at the level of the pons.[26] In phantom experiments, the slope of the profile curve for a vascular model of 3- to 4-mm diameter filled with contrast medium of sufficiently high attenuation became steeper with a smaller pixel size and using a "bone" kernel compared with a "standard" kernel (ie, increased spatial resolution).[27,28] In this study, this outcome might have led to a significant increase in the attenuation of the BA by MBIR, but we achieved adequate enhancement (eg, >250 HU) in the intracranial arteries even with FBP. With MBIR, the contrast-to-noise ratio increased significantly in the posterior fossa.

On volume-rendered images, all those advantages enhanced image quality and contributed to the significantly improved subjective delineation of all the brain arteries in the posterior fossa except the BA, by MBIR compared with FBP. We observed no significant difference in subjective delineation of the BA between FBP and MBIR, probably because the BA was the largest vessel and sufficiently delineated even with FBP. Actually, the mean visual evaluation score by both readers decreased in order from the BA and VA to the PICA to the SCA to the AICA by using both FBP and MBIR algorithms, and the scores for the BA by FBP were 3 or 4 in all patients except 1. By MBIR, the mean visual score was 3.0 or higher for all those arteries except the AICA (2.6 ± 0.7) as assessed by reader 1, and image quality was acceptable for arteries in the posterior fossa except 1

ture; in-plane resolution was comparable between MBIR and FBP with a "bone" kernel; and image noise was nearly 50% better by using MBIR than FBP with a "standard" kernel.[1] Among the 3 different reconstruction kernels, spatial resolution and image noise increase in

SCA for reader 1. On maximum intensity projection compared with volume-rendered imaging, improved vessel enhancement, contrast-to-noise ratio and sharpness of vessel contour, and reduced posterior fossa artifacts by MBIR were subjectively more prominent, particu-

larly in larger arteries such as the BA and VA. On maximum intensity projection, the average improvement of the visual score by MBIR compared with FBP was 0.84 for the BA and VA and 0.46 for the SCA, AICA, and PICA. Compared with FBP, MBIR significantly improved subjective delineation of all brain arteries in the posterior fossa, including the BA. The mean visual score by MBIR was 3.0 or higher for all those arteries except the AICA (2.8 ± 0.7 by both the readers), whereas the score by FBP was 3.0 or higher only for the BA and VA. Thus, MBIR may improve assessment of intracranial aneurysms, especially peripherally located aneurysms of the posterior fossa.

Our study was limited because it was retrospective and included only a small study population. A large-scale prospective study may be warranted to confirm our results. We did we not use DSA images of our patients as a reference for accurately defining the vessels assessed in this study. A final consideration is that we did not directly assess the diagnostic accuracy of intracranial aneurysms, especially in the posterior fossa. However, the close topographic proximity to the osseous structures of the skull base may still make arterial delineation and aneurysm detection challenging even if image quality is substantially improved in the posterior fossa. A further comparison study of diagnostic performance among different reconstruction algorithms and imaging techniques should be performed.

CONCLUSIONS

In CTA examinations of the head, MBIR is substantially better than FBP in delineating brain arteries in the posterior fossa that are smaller than the BA. Its use may lead to improved noninvasive detection of peripherally located aneurysms of the posterior fossa with CTA and may reasonably reduce radiation and contrast medium dose and contrast injection rate.

REFERENCES

1. Thibault JB, Sauer KD, Bouman CA, et al. **A three-dimensional statistical approach to improved image quality for multislice helical CT.** *Med Phys* 2007;34:4526–44
2. Velthuis BK, Rinkel GJ, Ramos LM, et al. **Subarachnoid hemorrhage: aneurysm detection and preoperative evaluation with CT angiography.** *Radiology* 1998;208:423–30
3. Schwartz RB, Tice HM, Hooten SM, et al. **Evaluation of cerebral aneurysms with helical CT: correlation with conventional angiography and MR angiography.** *Radiology* 1994;192:717–22
4. Vieco PT, Shuman WP, Alsofrom GF, et al. **Detection of circle of Willis aneurysms in patients with acute subarachnoid hemorrhage: a comparison of CT angiography and digital subtraction angiography.** *AJR Am J Roentgenol* 1995;165:425–30
5. Korogi Y, Takahashi M, Katada K, et al. **Intracranial aneurysms: detection with three-dimensional CT angiography with volume rendering—comparison with conventional angiographic and surgical findings.** *Radiology* 1999;211:497–506
6. Villablanca JP, Martin N, Jahan R, et al. **Volume-rendered helical computerized tomography angiography in the detection and characterization of intracranial aneurysms.** *J Neurosurg* 2000;93:254–64
7. Wiebers DO, Whisnant JP, Huston J 3rd, et al, for the International Study of Unruptured Intracranial Aneurysms Investigators. **Unruptured intracranial aneurysms: natural history, clinical outcome, and risks of surgical and endovascular treatment.** *Lancet* 2003;362:103–10
8. Ishibashi T, Murayama Y, Urashima M, et al. **Unruptured intracranial aneurysms: incidence of rupture and risk factors.** *Stroke* 2009; 40:313–16
9. Hashimoto H, Iida J, Hironaka Y, et al. **Use of spiral computerized tomography angiography in patients with subarachnoid hemorrhage in whom subtraction angiography did not reveal cerebral aneurysms.** *J Neurosurg* 2000;92:278–83
10. Kurokawa Y, Yonemasu Y, Kano H, et al. **The usefulness of 3D-CT angiography for the diagnosis of spontaneous vertebral artery dissection: report of two cases.** *Comput Med Imaging Graph* 2000;24:115–19
11. Mizushima H, Kobayashi N, Yoshiharu S, et al. **Aneurysm of the distal anterior inferior cerebellar artery at the medial branch: a case report and review of the literature.** *Surg Neurol* 1999;52:137–42
12. Carvi y Nievas MN, Haas E, Höllerhage HG, et al. **Complementary use of computed tomographic angiography in treatment planning for posterior fossa subarachnoid hemorrhage.** *Neurosurgery* 2002; 50:1283–88, discussion 1288–89
13. Iwanaga S, Shrier DA, Okawara SH, et al. **Value of CT angiography in the evaluation of a peripheral inferior cerebellar artery aneurysm: case report.** *Clin Imaging* 1999;23:77–80
14. Velthuis BK, Van Leeuwen MS, Witkamp TD, et al. **Computerized tomography angiography in patients with subarachnoid hemorrhage: from aneurysm detection to treatment without conventional angiography.** *J Neurosurg* 1999;91:761–67
15. Ertl-Wagner BB, Hoffmann RT, Bruning R, et al. **Multi-detector row CT angiography of the brain at various kilovoltage settings.** *Radiology* 2004;231:528–35
16. Ertl-Wagner B, Eftimov L, Blume J, et al. **Cranial CT with 64-, 16-, 4- and single-slice CT systems-comparison of image quality and posterior fossa artifacts in routine brain imaging with standard protocols.** *Eur Radiol* 2008;18:1720–26
17. Moström U, Ytterbergh C. **Artifacts in computed tomography of the posterior fossa: a comparative phantom study.** *J Comput Assist Tomogr* 1986;10:560–66
18. Rozeik C, Kotterer O, Preiss J, et al. **Cranial CT artifacts and gantry angulation.** *J Comput Assist Tomogr* 1991;15:381–86
19. Glover GH, Pelc NJ. **Nonlinear partial volume artifacts in x-ray computed tomography.** *Med Phys* 1980;7:238–48
20. Joseph PM, Spital RD. **A method for correcting bone induced artifacts in computed tomography scanners.** *J Comput Assist Tomogr* 1978;2:100–08
21. Herman GT. **Correction for beam hardening in computed tomography.** *Phys Med Biol* 1979;24:81–106
22. Herman GT. **Demonstration of beam hardening correction in computed tomography of the head.** *J Comput Assist Tomogr* 1979;3:373–78
23. Elbakri IA, Fessler JA. **Statistical image reconstruction for polyenergetic X-ray computed tomography.** *IEEE Trans Med Imaging* 2002; 21:89–99
24. Lin XZ, Miao F, Li JY, et al. **High-definition CT gemstone spectral imaging of the brain: initial results of selecting optimal monochromatic image for beam-hardening artifacts and image noise reduction.** *J Comput Assist Tomogr* 2011;35:294–97
25. Hsieh J, Molthen RC, Dawson CA, et al. **An iterative approach to the beam hardening correction in cone beam CT.** *Med Phys* 2000;27: 23–29
26. Smoker WR, Price MJ, Keyes WD, et al. **High-resolution computed tomography of the basilar artery. 1. Normal size and position** *AJNR Am J Neuroradiol* 1986;7:55–60
27. Suzuki S, Furui S, Kaminaga T. **Accuracy of automated CT angiography measurement of vascular diameter in phantoms: effect of size of display field of view, density of contrast medium, and wall thickness.** *AJR Am J Roentgenol* 2005;184:1940–44
28. Suzuki S, Furui S, Kaminaga T, et al. **Measurement of vascular diameter in vitro by automated software for CT angiography: effects of inner diameter, density of contrast medium, and convolution kernel.** *AJR Am J Roentgenol* 2004;182:1313–17